New Insights into Corrosion Mechanisms of Dense Refractory Castables Containing a Novel Calcium Aluminate Binder*

A. Borovsky, Chr. Parr, J.-M. Auvray, H. Fryda

Castable developments for steel ladles during the last three decades have been based around alumina-spinel and alumina-magnesia systems, which are often denominated as "preformed" spinel castables and "in-situ" castables, respectively. It has been shown that changing the microstructure of ladle castables can lead to improved resistance to corrosion. One approach to achieve this, has been the recent development of a novel Calcium Magnesium Aluminate (CMA) cement. This paper presents an analysis of corroded samples through optical and SEM image analysis. The investigation by microscopy gives a correlation between the thermomechanical properties from phase and particle distributions, microstructural features and glassy phases of the castables with corrosion mechanisms. Conclusions are drawn, from the established hypothesis, as to the supposed mechanism of corrosion and ways in which corrosion resistance using this novel CMA binder can be further optimised through formulation control. Thus, leading to the belief that monolithic refractories can be considered in constant evolution.

1 Introduction

Alumina-spinel, alumina-magnesia, and more recently, a hybrid combination of both castables [1], have been effectively used in refractory steel ladles, mainly due to their outstanding corrosion resistance to slag [2, 3]. The content of synthetic spinel or magnesia is a critical selection parameter for slag penetration and melt-corrosion development of the refractory material. According to the previous work of *Kanatani* and *Imaida* [4], a reasonable compromise between both requirements can be achieved in the castable containing between 20–40 % of magnesium aluminate spinel after firing. Another factor with a direct impact upon the penetration resistance of the refractory is the size of spinel grain [5]. Fine crystal sizes of spinel grains, as a result of their more homogeneous distribution throughout the castable matrix, enable the development of a dense microstructure, which proved to be responsible for the better slag penetration and corrosion resistance. They can also lead to a higher sintering reactivity of the refractory, which can, above a certain level, induce shrinkage [6]. Very fine spinel can be generated by adding magnesia which reacts with alumina fillers during firing to form in-situ spinel. This reaction is followed, among others, by volume expansion [7]. If the expansion is extensive it can induce stresses that can ultimately lead to peeling-type crack initiation. To improve the volume stability of the castable, a small amount of microsilica is often added to the dry-mix [3, 8] although the microsilica addition reduces the castable strength at the operating temperature [9]. Therefore, the castable design should be tailored to offer a balance between expansion and sintering reactivity.

A novel calcium magnesium aluminate (CMA) cement enables formulators to achieve the needed balance and customize precise properties of their refractory castables. Investigations of this new CMA binder in different types of ladle castables have shown that such castables better resist a large range of slag compositions [10]. The basis of CMA is a unique multiphase clinker with a microstructure of calcium aluminate phases embedded in a matrix of microcrystalline magnesium aluminate spinel crystals. The aim of this paper is to present analyses of corroded and non-corroded samples, and to find a correlation between thermomechanical properties of the castables, and their microstructure with focus on the mechanisms that are basic to the corrosion of castables.

Adriana Borovsky
Kerneos do Brasil Ltda
722-030 São Goncalo RJ
Brasil

Chris Parr, Jean-Michel Auvray, Hervé Fryda
92521 Neuilly sur Seine
France

Corresponding author: *Adriana Borovsky*
E-mail: Adriana.Borovsky@kerneos.com

Keywords: corrosion mechanism, CMA, calcium aluminate, microstructure, refractory castables, alumina-spinel, alumina-magnesia, spinel, CA_6
Received: 27.11.2012
Accepted: 21.12.2012

* The paper was presented at ALAFAR in Cancún/MX in Nov. 2012 and was awarded with the 2nd prize of the ALAFAR Award 2012

Tab. 1 Chemical and mineralogical compositions [mass-%]

Chemistry	Al_2O_3	CaO	MgO	SiO_2
Secar®71	68,7–70,5	28,5–30,5	<0,5	0,2–0,6
CMA 72	69–71	8–11	16–22	<1,0
Mineralogy	**CA**	**CA_2**	**MA**	**C_2AS**
Secar®71	56–61	39–44	0	<1
CMA 72	18–22	8–12	68–72	<1

2 Experimental

2.1 Material and test methods

The chemical and mineralogical compositions of calcium aluminate cement (CAC) and CMA was determined by X-ray techniques are shown in Tab. 1.

Both binders have a Blaine specific surface area close to 4000 cm^2/g with a median grain size d_{50} of 15–18 µm, measured with a laser granulometer. Tab. 2 shows compositions of model castables used in this study. MA1 and MA2 systems contain pre-reacted sintered spinel. M1 and M2 are formulated with free sintered MgO (Periclase). M2 is a hybrid system as it contains both MgO and MA spinel through the presence of the CMA cement. The formulation logic is to maintain the chemical composition of the castable and the same total MA phase after sintering. The total amount of binder has been chosen to ensure that these castables are low cement castables (LCC) with a constant CaO content of 1,7 % as indicated in Tab. 2.

A polycarboxylate ether based additive, Peramin AL200, was chosen to efficiently deflocculate the castables at a very low amount of mixing water.

The corrosion and penetration resistance against a BOF slag (slag B) was tested in a laboratory scale rotary kiln according to ASTM C874-99. The composition of this slag is shown in Tab. 3. Slag resistance and some other properties at high temperature for these materials have been already discussed elsewhere [10].

Microstructure analyses have been performed with a scanning electron microscope (SEM) using backscattered images on polished surfaces. The chemical compositions of the phases have been studied using energy dispersive spectroscopy (EDS). The samples have been taken from specimens that were pre-fired during 5 h at 1550 °C and then exposed to an iron rich slag in a laboratory rotary kiln at 1550 °C.

Tab. 2 Composition of alumina-spinel (MA) and alumina-magnesia (M) model castables [mass-%] and estimation of their chemical composition

Castable	MA1	MA2	M1	M2
Binder System	**CAC**	**CMA**	**CAC**	**CMA**
Tabular alumina 0–6 mm	60	61	75,5	70
Reactive alumina	11	11	11	8
Sintered spinel 0–1 mm	13	10		
Sintered spinel <90 µm	10			
Sintered MgO <74 µm			6,5	3
CAC (SECAR® 71)	6		6	
CMA (CMA 72)		18		18
Silica (Elkem Microsilica® 971U)			1	1
PCE (Peramin®AL 200)	+0,1	+0,1	+0,15	+0,1
Water	+4	+4	+4,5	+4,5
MA	23	23	23	23
CaO	1,7	1,7	1,7	1,7
MgO total	5,2	5,8	6,5	6,6
Al_2O_3	93,1	92,4	90,8	90,6
SiO_2			1,0	1.0
Total	100	100	100	100

Tab. 3 BOF slag composition (slag B)

[mass-%]	Al_2O_3	SiO_2	FeO	MnO	CaO	MgO	C/S
Slag B	2	15	19	6	53	5	3,5

3 Results and discussion

3.1 Microstructural analyses of non-corroded castables

SEM images of the non-corroded materials are shown in Fig. 1. The microstructure of alumina-spinel castable with CAC (Fig. 1a) is represented by a porous matrix embedding tabular alumina (TA) and spinel (MA) aggregates, and interlocking calcium hexa-aluminate ($CaO{\cdot}6Al_2O_3$ – formed due to the reactions and transformation of CAC) crystals and fine spinel grains. Porous clusters of CA_6 needles are plentiful at the edge of TA aggregates and in the castable's matrix but are also visible at the border of MA grains. The CA_6 needles have a length of 10–20 µm and thickness of 0,5–1,0 µm.

The microstructure of the same castable but formulated with CMA, shown in Fig. 1b, presents a picture of uniformly distributed very fine spinel grains and needles of CA_6 almost as if sintered together into a dense matrix. The CA_6 needles are slightly shorter and thicker than the ones observed in MA1 castable. Furthermore, in the SEM image of Fig. 1b, a stronger interlocking bond between TA, and also MA aggregates, and the matrix is clearly visible. Fig. 1c shows the microstructure of alumina magnesia castable with CAC. In this case, the CA_6 phase has been found predominantly at the boundaries of TA aggregates and grew to a plate morphology. The shortage of CA_6 phase in the matrix can be attributed to the lack of available alumina used up for the generation of in-situ spinel. Conversely, in a more dense microstructure of alumina-magnesium castable formulated with CMA, as shown in Fig. 1d, different CA_6

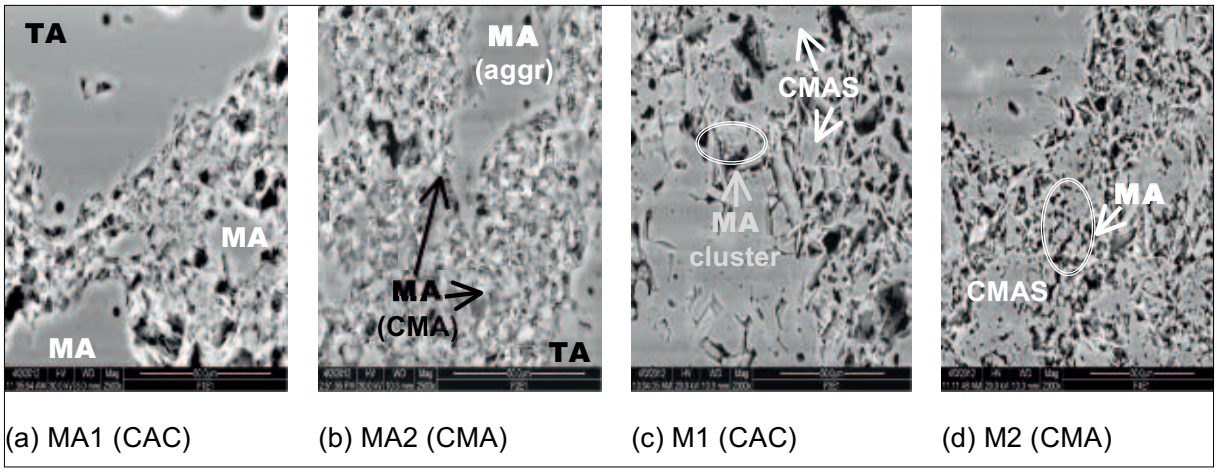

Fig. 1a–d SEM images of non-corroded alumina-spinel castables (MA) and alumina-magnesium castables (M) after firing at 1550 °C

phase location and morphology is observed. The bonding matrix between TA aggregates is mainly constituted of acicular CA_6 crystals at the TA boundaries while coupled crystalline CA_6 platelets are homogeneously distributed throughout the microstructure and bridging fine spinel particles from CMA and also from in-situ formation. It can be also observed in Fig. 1d that the fine spinel grains remain well distinguished from other constituents of the matrix. The addition of polycarboxylate ether based additive has probably contributed to a greater occurrence of coupled CA_6 platelets in both alumina-magnesium castables formulated with CAC and CMA by modifying porosity of the castable microstructure and the extension of contact areas between alumina and calcium source, and therefore between alumina and calcium dialuminate. This detected variety in CA_6 morphology and distribution suggests possibilities of mastering reaction routes to tailor their shape and growth.

3.2 Microstructural analyses of corroded castables

SEM images of the microstructures, developed in alumina-spinel castables formulated with CAC and CMA after corrosion tests, are shown in Fig. 2. An altered layer with a thickness of approximately 500 µm, as a result of the slag penetration into the MA1 castable, is visible in Fig. 2a. The progressive degradation of the refractory material and continuous infiltration, and diffusion of the slag (systematically replaced by fresh slag) led to the phase transformation, and formation of new calcium aluminate based multi-oxide phase assemblages containing some slag elements, such as Fe, Mn and Si. In particular, a solid phase zone with an elongated shape in silica-lime rich liquid is the most noticeable. EDS analyses revealed a variety of compositions derived from CA_2 within the elongated zones (points 1 and 2, Tab. 4).

Moreover, some fine spinel grains from the matrix randomly distributed throughout the altered layer after the slag attack, are also visible (Fig. 2a iii). An example of interaction between a coarse spinel aggregate and slag is given in Fig. 2a ii. Microstructural analyses indicate that the slag penetration occurs along matrix grain boundaries and via the interconnected porosity and confirm the interaction between the slag and components of the castable (TA + matrix). This interaction shows the typical pattern of a dissolution-precipitation mechanism with progressive dissolution of alumina and spinel, followed by precipitation of new calcium aluminate phases enriched in silica and iron from the reaction with calcia from the slag. In MA2 (CMA), the interface between the altered layer with a thickness of approximately 400 µm and the refractory material, is very clear (Fig. 2b i). The penetration of the slag and its interaction with the castable resulted in the formation of calcium-aluminate-ferrite crystals elongated in shape and with a stoichiometry derived from CA_2 (point 4). The surrounding glassy phase (point 5) contains less iron than MA1 castable. The higher magnification micrograph (Fig. 2b ii) revealed that these elongated crystals act as a barrier against the further slag penetration. The interface between the slag and a TA aggregate consists of 3 mono-mineral layers derived from CA_6, CA_2 and CA successively (Fig. 2b iii). Therefore, a change in the chemical composition and/or viscosity of molten slag resulting from a more homogeneous distribution of fine spinel particles and consequently, a higher absorption of the metallic cations, such as Fe^{2+}, Fe^{3+} and Mn^{2+}, contribute to the higher corrosion resistance of CMA-based castable.

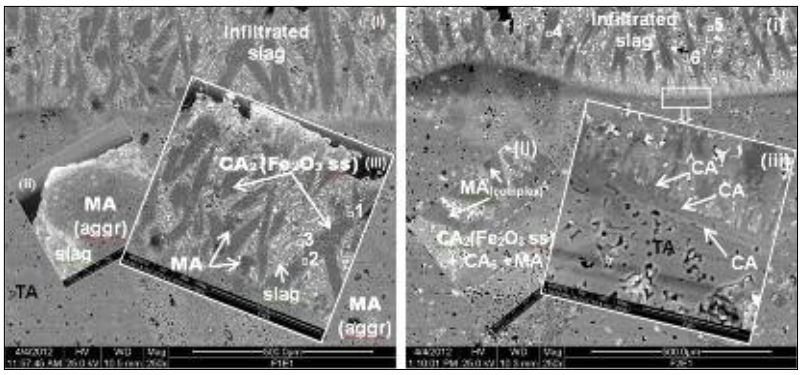

Fig. 2a-b SEM images of the corroded alumina-spinel castables: (a) MA1 (CAC) and (b) MA2 (CMA)

Tab. 4 EDS analyses [mass-%] of the corroded castables

	1	2	3	4	5	6	7	8	9	10	11	12
O	46,6	46,9	44,3	48,9	46,0	41,7	46,8	43,1	48,2	49,2	46,3	44,1
Mg	6,7	0	0	0	0	0	0	0	10,1	0,3	0	0
Al	32,1	35,1	17,2	34,8	18,9	11,5	36,5	17,0	33,1	44,4	38,3	21,8
Ca	6,5	14,7	25,1	13,5	25,1	25,4	14,4	25,2	5,6	5,7	14,3	25,1
Si	0,7	0,6	7,1	0,3	6,7	1,3	0	6,4	0,30	0,4	0	5,9
Mn	2,2	0,3	0,6	0	0	4,4	0	1,2	0,65	0	0	0
Fe	5,2	2,4	5,7	2,5	3,3	15,7	2,30	7,1	2,05	0	1,1	3,1

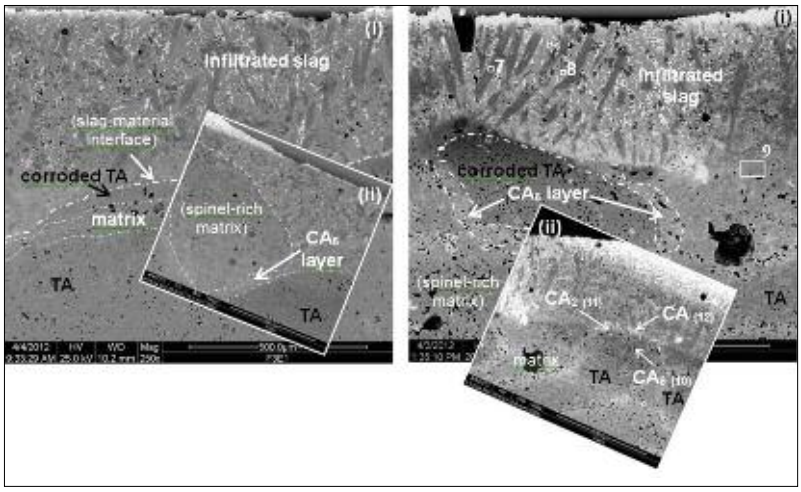

Fig. 3a–b SEM images of the corroded alumina-magnesium castables: (a) M1 (CAC) and (b) M2 (CMA)

Fig. 3 shows microstructures of the corroded alumina-magnesia castables. Generally speaking, the microstructures of the infiltrated layers for both materials are quite similar to those observed for the alumina-spinel castables, except for some very fine spinel containing zones. One can also notice that the slag-refractory interfaces are not that well pronounced. The altered layer of M1 castable has a thickness of approximately 500 µm (Fig. 3a i) while the layer of M2 castable with CMA is only about 380 µm thick (Fig. 3b i). A strong interlocking network between CA_6 and microcrystalline spinel grains, associated to a denser microstructure, limits a further infiltration of the slag (point 9).

4 Conclusions

The microstructure of non-corroded and corroded alumina-spinel and alumina-magnesium castables after a corrosion test using a rotary furnace has been studied. The following conclusions can be drawn from the present study that explain higher corrosion resistance and lower slag penetration of CMA based castables.

- The slag penetrates into the castable by partially dissolving alumina from TA aggregates and CA_6 from the matrix.
- New calcium aluminate phases with some elements from the slag (Fe, Si) are formed inside a CaO-rich layer (elongated crystals CA_2 and CAS liq).
- Homogeneously distributed microcrystalline spinel is more resistant to a progressive slag attack by incorporating Fe and Mn elements, and thus changing the composition, and viscosity of the liquid phase inside the altered layer.
- The slag/refractory interface consists of a succession of mono-mineral layers. The TA aggregates are surrounded by a CA_6 layer acting as a diffusion barrier.

References

[1] Dott, K.H.: Monolithic ladle lining at SSAB Tunnplåt in Luleå, Sweden. RHI Bulletin 1 (2008) 34–37

[2] Yamamura, T.; et al.: Development of alumina-spinel castables for steel ladles. Taikabutsu **42** (1990) [8] 427–434

[3] H. Naaby; et al.: Refractory wear mechanisms and influence on metallurgy. 37th Int. Coll. on Refractories, Aachen 1994, 198–204

[4] T. Kanatani, Y. Imaiida: Application of an alumina-spinel castable to the teeming ladle for stainless steelmaking. UNITECR'93 (1993), 1255–1266

[5] Nakashima, M.; Isobe, T.; Itose, S.: Improvement in corrosion of alumina-spinel castable by adding ultrafine spinel powder. Taikabutsu **52** (2000) [2] 65–72

[6] Bhatnagar, V.; Mukhopadhyay S.; Natarajan, C.: Development of improved quality spinel castable for steel ladle bottom. UNITECR'05 (2005) 162–166

[7] Braulio, M.A.L.; et al.: Expansion behaviour of cement bonded alumina-magnesia refractory castables. Amer. Ceram Soc. Bull. **86** (2007) [12] 9201–9206

[8] Bier, T.; et al.: Spinel forming castables: Physical and chemical mechanisms during drying. Refractories Application **4** (2000) 3–4

[9] Ko, Y.C.: Development and production of Al2O3-MgO and Al2O3-spinel castables for steel ladles. Mining and Metallurgy, Taipei, 47, 1, 132–140.

[10] Wöhrmeyer, C.; et al.: New spinel containing calcium aluminate cement for corrosion resistant castables. UNITECR'11 (2011) 1255–1266